*Supported by the Office of Naval Research.

[1]D. A. Micha, S. Y. Tang, and E. E. Muschlitz, Jr., Chem. Phys. Letters 8, 587 (1971).
[2]R. E. Olson, Chem. Phys. Letters 13, 307 (1972).
[3]E. E. Benton, E. E. Ferguson, F. A. Matsen, and W. W. Robertson, Phys. Rev. 128, 206 (1962).
[4]W. P. Sholette and E. E. Muschlitz, Jr., J. Chem. Phys. 36, 3368 (1962).
[5]D. A. MacLennan, Phys. Rev. 148, 218 (1966).
[6]C. R. Jones and W. W. Robertson, J. Chem. Phys. 49, 4240 (1968).
[7]A. L. Schmeltekopf and F. C. Fehsenfeld, J. Chem. Phys. 53, 3173 (1970).
[8]R. C. Bolden, R. S. Hemsworth, M. J. Shaw, and N. D. Twiddy, J. Phys. B 3, 61 (1970).
[9]J. T. Moseley, J. R. Peterson, D. C. Lorents, and M. Hollstein, preceding paper, Phys. Rev. A 6, 1025 (1972).
[10]S. Y. Tang, A. B. Marcus, and E. E. Muschlitz, Jr., J. Chem. Phys. 56, 1347 (1972).
[11]W. H. Miller, J. Chem. Phys. 52, 3563 (1970).
[12]W. H. Miller, C. A. Slocomb, and H. F. Schaefer, III, J. Chem. Phys. 56, 1347 (1972)..
[13]K. L. Bell, J. Phys. B 3, 1308 (1970).
[14]H. Fujii, H. Nakamura, and M. Mori, J. Phys. Soc. Japan 29, 1030 (1970).
[15]H. Hotop and A. Niehaus, Z. Physik 238, 452 (1970).
[16]A. A. Abrahamson, Phys. Rev. 178, 76 (1969).
[17]F. T. Smith, R. P. Marchi, W. Aberth, D. C. Lorents, and O. Heinz, Phys. Rev. 161, 31 (1967).
[18]E. W. Rothe, R. H. Neynaber, and S. M. Trujillo, J. Chem. Phys. 42, 3310 (1965).
[19]K. L. Bell, A. Dalgarno, and A. E. Kingston, J. Phys. B 1, 18 (1968).

PHYSICAL REVIEW A VOLUME 6, NUMBER 3 SEPTEMBER 1972

Optical Excitation and Polarization in Low-Energy Collisions of $He^+ + H_2$ †

R. C. Isler and R. D. Nathan
Department of Physics, University of Florida, Gainesville, Florida 32601
(Received 13 March 1972)

Optical studies of spectral lines produced in collisions of $He^+ + H_2$ have been made at energies below 700 eV. Lines of atomic hydrogen and helium are the only features observed. Emission cross sections have been measured for Lyman-β, Balmer-α, Balmer-β, and for the following He I lines: 5876 Å ($3\,^3D \rightarrow 2\,^3P$), 6678 Å ($3\,^1D \rightarrow 2\,^1P$), 4471 Å ($4\,^3D \rightarrow 2\,^3P$). Emission cross sections are also listed at certain selected energies for all spectral lines which have been observed. Polarization measurements have been performed on the Balmer-α, the Balmer-β, and the visible helium lines. Only the Balmer-α line exhibits significant polarization, and the results have been interpreted as indicating that the excited hydrogen atoms dissociate primarily in a direction perpendicular to the ion beam.

I. INTRODUCTION

Stedeford and Hasted[1] have measured the total cross section for charge transfer in $He^+ + H_2$ collisions and have tentatively postulated that the products are helium atoms in the ground state and H_2^+ ions in the lowest antibonding state. This state of the molecular ion, $2p\sigma_u$, dissociates into a proton and a hydrogen atom in the ground state. However, Dunn, Geballe, and Pretzer[2] have concluded from the shape and magnitude of the excitation cross section for producing the Lyman-α line by these collisions that the charge transfer at energies below 2.5 keV takes place almost 50% of the time into states of H_2^+ which then dissociate into a proton and a hydrogen atom in the $2\,^2P$ state. Gusev *et al.*[3] have shown that the Balmer-α and -β lines are also produced rather strongly by $He^+ + H_2$ collisions. The implications of these optical observations are that most, if not all, of the charge exchange at low energies takes place into states which ultimately result in excited hydrogen atoms. In the present work we have extended the spectral observations in order to obtain a more complete picture of the excited atomic states which may result from collisions of the $He^+ + H_2$ system at energies below 700 eV. Both the Lyman and Balmer series as well as lines of He I have been investigated. The emission cross sections for several lines have been measured from threshold to 700 eV, and values are tabulated at a few selected energies for all spectral features which have been observed.

The polarizations of the Balmer-α and -β lines have also been measured as a function of the energy of He^+ ions.[4] The latter appears to be unpolarized, but the former exhibits a polarization which is highly dependent upon the ion energy, being a maximum of about 12% at 50 eV. Van Brunt and Zare[5] have pointed out that both unequal populations of the magnetic substates and a nonisotropic angular distribution of the molecular dissociation axes are required in order for polarized light to be observed. Although the magnitude of the polarization can provide information about this angular distribution, the interpretation of the experimental results is ambiguous unless one knows which states

of the molecule (H_2^+) are preferentially populated and how these states are correlated to the magnetic sublevels of the dissociated atoms. Some of these ambiguities have been resolved by performing depolarization measurements (the Hanle effect) which show that the $3\,^2D \rightarrow 2\,^2P$ component of the Balmer-α line is the source of the polarized intensity at 50 eV. An additional inference based upon the uniformly decreasing intensities of the members of the Lyman and Balmer series is used to determine that the molecular dissociation occurs most probably in a direction normal to the incident ion beam.

II. APPARATUS

The ion-beam apparatus which has been used for the present work consists of three differentially pumped sections as shown in Fig. 1. The lower section is separated from the middle one by an electrically isolated chamber in which ions are made by electron bombardment. A set of electrostatic lenses in the center section is used to steer and focus the beam into the uppermost section which functions as a collision chamber. The base pressure of the system is 2×10^{-6} Torr.

The electron bombardment source utilizes an oxide cathode deposited on a grade-A nickel base which is 1.7 cm in diameter. Six tungsten filaments are employed to heat the cathode indirectly to temperatures up to 1000 °C. The nickel bases are cleaned chemically and hydrogen-fired before being sprayed with 15–30 mg of an RCA triple carbonate (Ba, Sr, Ca) mixture. While maintaining a pressure of 10^{-2} Torr of H_2 in the source chamber, the carbonates are converted to oxides at around 900 °C. Emission is obtained briefly at this temperature and then stabilized by drawing up to 300 mA for 3 h at 800 °C.

The emission of the cathode in a helium atmosphere is much less than it is in the hydrogen atmosphere under which the conversion takes place. Electron currents reach only 1–6 mA during the production of helium ions which are made by bombarding gas at a pressure of 2.5×10^{-4} Torr with electrons that have energies of less than 50 eV, thereby insuring that doubly charged ions or singly charged ions in the metastable state are not produced. The efficiency of production is enhanced, however, by means of a small coil which produces a strongly converging magnetic field in the region of the extraction aperature. The maximum field is about 100 G and is sufficient both to concentrate part of the electron flux and to guide the ions toward the aperture where they are drawn out by a potential difference of 2–5 eV into the buffer chamber which contains the electrostatic lenses. Ion currents range from 0.1 to 2.0 μA depending upon electron current and beam energies, and the spread in the beam energy is about 3.5 eV.

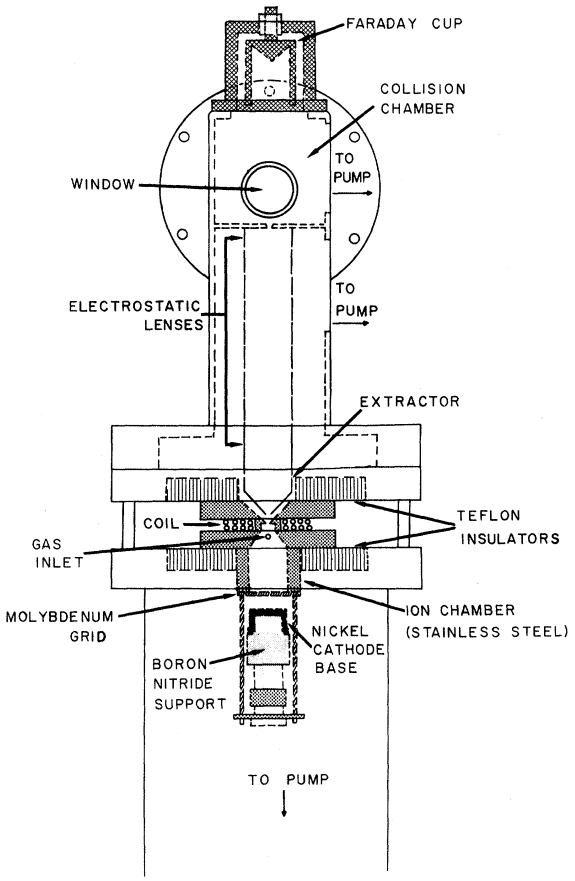

FIG. 1. Schematic diagram of apparatus.

The radiation produced in the collision chamber is observed at 90° to the beam direction. Two monochromators have usually been used to obtain spectral resolution: a Jarrell-Ash model 82-410 0.25-m instrument for the visible region and a McPherson model 225 for the vacuum ultraviolet region. All of the cross sections investigated appear to be linear functions of pressure up to 7×10^{-4} Torr, and the pressure of the target gas in the collision chamber is always kept below this value.

The apparatus has been designed so that the beam is oriented vertically, parallel to the entrance slit of the vacuum monochromator. However, it has been found that the relative cross-section curves obtained using this geometry are sometimes distorted owing to the variation in beam diameter as a function of energy and a corresponding change in the collection efficiency for the radiation emitted from a given segment of the beam. Therefore, it has been necessary to normalize the measurements of the Lyman-β cross sections at all energies by making comparison to the Lyman-α intensity and relating this intensity to the absolute mea-

surements of previous investigations.[2]

Negligible distortions of the cross-section curves occur if the beam has a small diameter compared to the slit length and if it is moving transverse to the slit. The visible lines were investigated using this arrangement because the 0.25-m monochromator can easily be placed in any orientation. Absolute cross sections were established by measuring the system response with a calibrated tungsten filament lamp then using the value for Balmer-α excitation at 150 eV given by Gusev *et al.*[3] Single-photon counting techniques are used in all experiments, but the signal is converted to analog form when recording spectral scans.

A cooled EMI 9558Q photomultiplier tube is employed for detection of visible lines, and a Bendix model 306 electron multiplier with a tungsten cathode is used for the vacuum ultraviolet emissions. The Bendix detector has a dark counting rate of about 3/min, and by employing a magnetic deflector to reduce the electron dark current from the unused portion of the cathode, the EMI tube achieves a noise rate of about 4/sec.

Narrow-band filters are used to isolate the Balmer-α and -β lines when making polarization measurements. The relative intensities of light emitted with electric field vectors parallel to and perpendicular to the beam axis are determined by using a polarizing film which rejects more than 98% of the undesired component. A pair of 8-in.-diam Helmholtz coils are placed around the collision chamber with the magnetic field applied along the direction of observation in order to observe the Hanle effect.

III. SPECTRA AND EXCITATION CROSS SECTIONS

Spectral scans made at 25-Å resolution in the visible region are shown in Fig. 2 for beam energies of 200 and 700 eV. The Balmer lines completely dominate all other spectral features at the lower energy and five members of the series are clearly visible in the spectrum. The line at 3889 Å is a combination of the sixth member of the series and a line of He I. The data obtained at a beam energy of 700 eV show that several lines of He I are also seen quite prominently, indicating a rapid rise of the probability of charge exchange into excited states as the energy is increased. A portion of the far-ultraviolet spectrum extending from about 500 up to 1300 Å is shown in Fig. 3. This spectrum has been obtained at a bombarding energy of 500 eV. The Lyman-α line is much more intense than the other members of the series and only the first one of the resonance lines of helium shows up strongly above the background. Radiation from excited states of H_2^+ to the electronic ground state might also be expected to appear in this vacuum ultraviolet region, but so far we have been unable to detect such transitions.

The emission cross sections of the observed hydrogen and helium lines are listed in Table I for 500-eV bombarding energy for the ultraviolet lines and 700-eV bombarding energy for the visible lines. Cross sections as a function of energy are plotted in Figs. 4 and 5 for several of these transitions. In all of our experiments we have made only relative intensity measurements, and the error bars represent 1 standard deviation of the number of counts recorded at a particular energy.

Absolute cross sections have been computed for the Lyman series by comparing relative intensities to the absolute measurements of Dunn, Geballe, and Pretzer at all energies.[2] The relative response of the monochromator and detector to radiation at 1216 Å and to radiation at the wavelengths of the higher lines of the Lyman series has been obtained by measuring the intensities of two lines of O I which originate on the $2p^3(^2P^0)3s''\,^1P^0$ state and decay to either the $2p^4\,^1S$ or $2p^4\,^1D$ states of the ground configuration.[6] These lines are at 1217 and 999 Å, respectively. It was assumed that the system response to all members of the Lyman series other than Ly-α was the same as that which was measured at 999 Å. It is estimated that this assumption may lead to errors of about 10% in the cross sections of these lines relative to the Lyman-α line.

It should also be pointed out that there is some question about the cross section reported by Dunn, Geballe, and Pretzer for Lyman-α at low energies. Young, Stebbings, and McGowan[7] have made similar measurements at 54.5° to the beam direction rather than at 90° in order to eliminate uncertainties which can arise in the measurements of cross sections if the radiation is polarized. At high energies, above 1 keV, the two results were in good agreement. Below this energy, though, Young *et al.* obtained cross sections higher than the value measured by the other group. Rather than attributing the discrepancy to the effects of polarization, they believed that certain geometrical effects were not properly taken into account in the experiment of Dunn *et al.* In view of the present results which show that the Balmer-α radiation can be polarized, it seems reasonable to expect that the Lyman-α line may also be polarized at low energies, and that discrepancies in the two measurements of absolute cross sections should be apparent from this effect as well as from differences in geometry. However, because the measurements made by Young *et al.* do not extend below 500 eV we have used the other results to normalize our data. It would be preferable in our experiments to choose a single point at which the previous two sets of measurements are in near agreement and then to perform our own relative

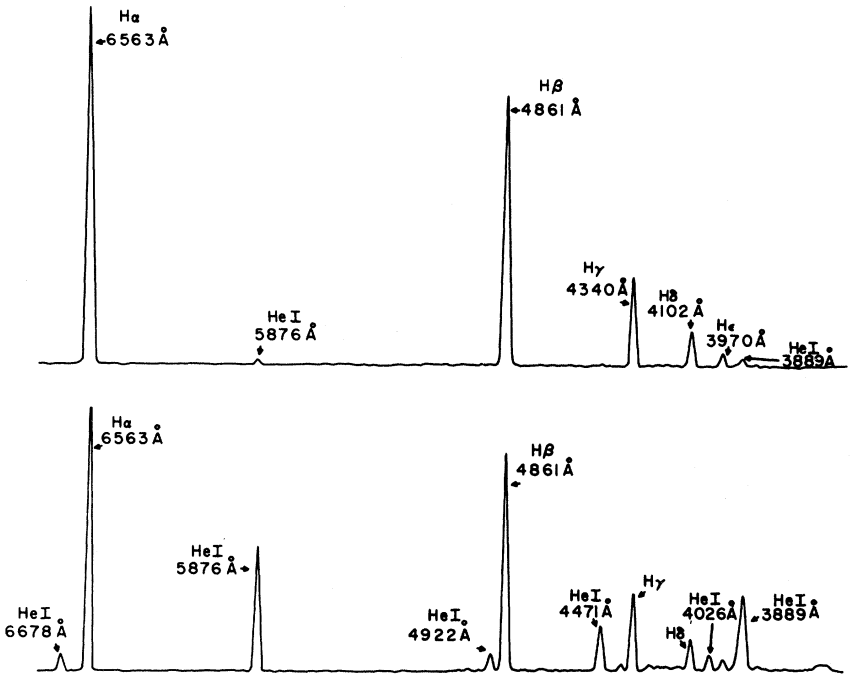

FIG. 2. Visible spectra produced by $He^+ + H_2$ collisions. The upper and lower scans were produced at ion energies of 200 and 700 eV, respectively.

measurements of Lyman-α as a function of energy rather than comparing our results for Lyman-β point by point with those of Dunn *et al.* However, as discussed in the preceding section, this procedure cannot be carried out reliably with the present apparatus. The cross sections for producing both the Lyman and Balmar lines are qualitatively similar, rising monotonically from threshold to maxima between 150 and 300 eV. All of these lines become visible above the background at energies between 30 and 50 eV. The helium lines appear to have slightly higher thresholds but do not peak at energies below 700 eV; however, there is a noticeable shoulder around 100 eV in the cross sections for the triplet lines which could indicate that crossings of potential surfaces are involved in the charge exchange process. This shoulder is not apparent in the cross section of the 6678-Å singlet line, but counting rates for this line at energies below 200 eV are less than the photomultiplier dark count rate, and uncertainties in the cross sections are subsequently large.

Dunn *et al.* have discussed the possible mechanisms which could lead to the production of Lyman-

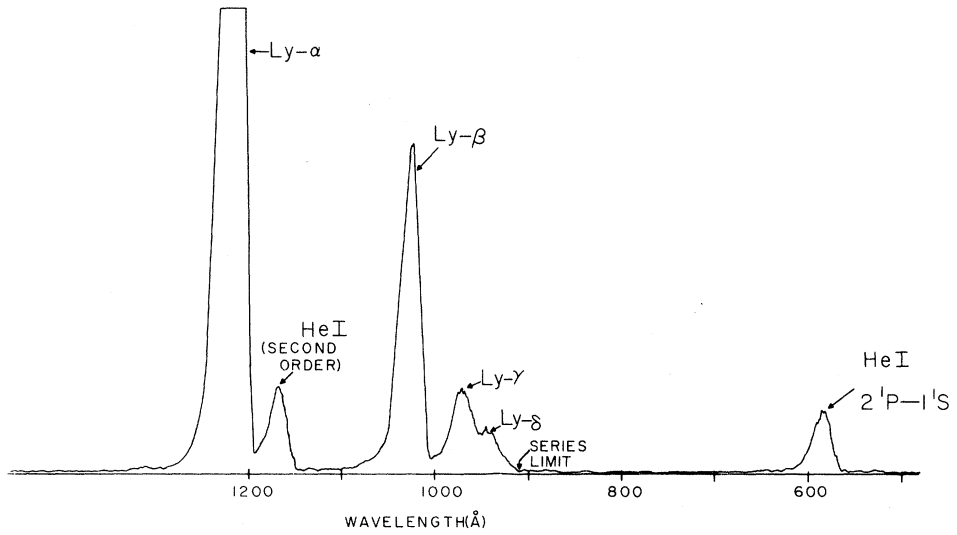

FIG. 3. Far-ultraviolet spectrum from $He^+ + H_2$ collisions at an ion energy of 500 eV.

α radiation and concluded that the most likely of these is charge exchange into the ground state of helium leaving an excited H_2^+ molecules which then dissociates into an excited hydrogen atom and a proton. The most convincing arguments for this conclusion are that the total charge-exchange cross section is very similar in shape to the Lyman-α cross section and that both curves exhibit a peak of about 300 eV, the emission cross section being about 42% that for total charge exchange at this point. It can be seen from Table I and Fig. 4, that about an additional 12% (cascading cannot be taken into account here because the populations of the various orbital states are not known) of the total charge transfer can be due to processes which leave H_2^+ in states which dissociate into protons and hydrogen atoms with $n \geq 2$. In view of the possibility that the Lyman-α cross section measured by Dunn *et al.* may in fact be smaller than the actual cross section at low energies and that excitation into the 2*S* state of hydrogen cannot be detected optically, the entire charge-transfer cross section for the $H_2 + He^+$ system at low energies might well take place by producing states of H_2^+ which dissociate into an excited atom and a proton.

Similar cases in which the charge transfer takes place mainly through excited states are known for certain ion-atom systems and can be understood from the crossing of diabatic potential curves of the quasimolecule. For example, Smith, Fleischmann, and Young[8] have discussed these potential curves for the $(HeAr)^+$ system. At large nuclear separations the energy of the $He^+ + Ar$ complex is higher than that of $He + Ar^+$ but lower than that of $He + (Ar^+)^*$. As the helium ion approaches the argon atom the potential curve rises steeply, cross-

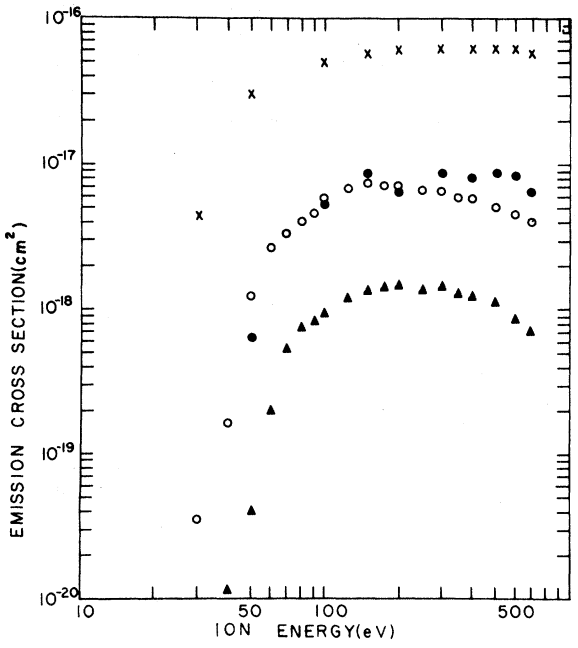

FIG. 4. Emission cross sections of hydrogen lines; crosses, Ly-α; solid circles, Ly-β; open circles, H_α; triangles, H_β. The data for the Ly-α line are taken from Ref. 2.

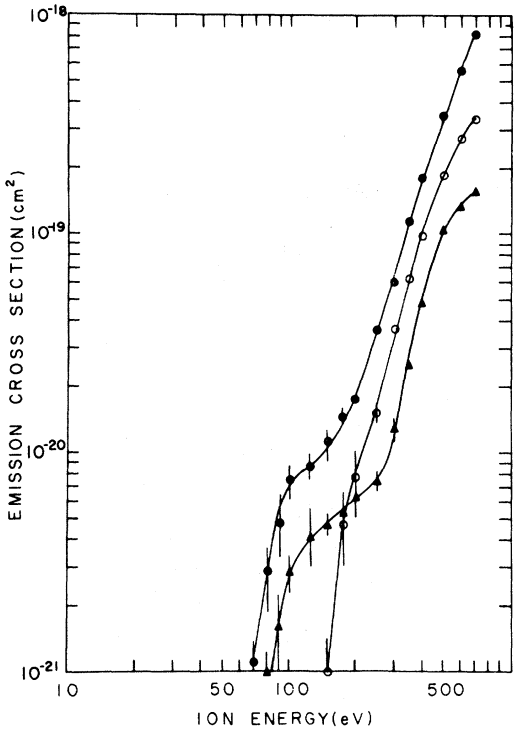

FIG. 5. Emission cross sections of helium lines; solid circles, 5876 Å ($3\,^3D \rightarrow 2\,^3P$); open circles, 6678 Å ($3\,^1D \rightarrow 2\,^1P$); solid triangles, 4471 Å ($4\,^3D \rightarrow 2\,^3P$).

TABLE I. Emission cross sections for observed lines of hydrogen and helium. Uncertainties in relative cross sections are estimated to be 10% or less.

Beam energy (eV)	Emitting species	Transition	Cross section (10^{-18} cm^2)
500	Hydrogen	Ly-α	65.0
		Ly-β	9.0
		Ly-γ	2.2
		Ly-δ	1.2
700	Hydrogen	H_α	4.11
		H_β	0.72
		H_γ	0.27
		H_δ	0.13
		H_ϵ	0.05
700	Helium	6678 Å ($3\,^1D \rightarrow 2\,^1P$)	0.34
		5876 Å ($3\,^3D \rightarrow 2\,^3P$)	0.83
		4921 Å ($4\,^1D \rightarrow 2\,^1P$)	0.06
		4471 Å ($4\,^3D \rightarrow 2\,^3P$)	0.16
		4387 Å ($5\,^1D \rightarrow 2\,^1P$)	0.02
		4026 Å ($5\,^3D \rightarrow 2\,^3P$)	0.07
		5015 Å ($3\,^1P \rightarrow 2\,^1S$)	0.01
		3889 Å ($3\,^3P \rightarrow 2\,^3S$)	0.28
		7065 Å ($3\,^3S \rightarrow 2\,^3P$)	0.22

ing the potential curves for neutral helium in the ground state and excited argon ions at internuclear distances larger than that at which it crosses the potential curves that lead to argon ions in the ground state. Hence, a large fraction of the charge exchange, particularly at low energies, may take place through excited states.

Although the $(HeH_2)^+$ system is more complicated than the ion-atom complex, it is possible that a similar model may explain the apparent dominance of charge-transfer processes which leave excited molecular ions as products. The asymptotic internal energy of the $He^+ + H_2$ system before collision exceeds that of the final state, $H + H^+ + He$, by 6.6 eV, but is less than the final state $H^*(2P) + H^+ + He$ by 3.6 eV. The potential surface of this system is likely to become more strongly repulsive as the ion approaches the molecule and it would appear that at low energies it could diabatically cross the surfaces which lead to excited hydrogen atoms in the product but not necessarily cross the surface leading to hydrogen in the ground state.

IV. POLARIZATION MEASUREMENTS

Several experiments have demonstrated that polarized radiation is produced by collisions of electrons[9] and ions[10] with molecular hydrogen. We have shown previously that the H_α line produced in $He^+ + H_2$ collisions is polarized and that the polarization is strongly dependent upon the bombardment energy.[4] This dependence is shown in Fig. 6 together with the measured polarization of the H_β line. The polarization of the latter, as well as that of the He I lines, is small and does not exhibit the marked variation with collision energy that the former does. Although polarization measurements are required in order to correct the computed emission cross sections presented in Sec. III, such measurements may be even more important because of their potential for providing insight into the collisional mechanisms of the dissociative charge-exchange process.

Van Brunt and Zare[5] have pointed out that the polarization of light emitted by atoms which are produced by molecular dissociation can be related to the angular distribution of the dissociation axes. It is necessary that the angular distribution be nonisotropic and that the magnetic substates of the upper state of the spectral line observed be unequally populated in order to produce polarized light. Unfortunately, the observed polarization and the angular distribution cannot be related unambiguously unless one knows the relative populations of the magnetic substates. Also, the fact that the observed hydrogenic lines are combinations of transitions which originate from different terms makes the analysis more difficult than it would be for other atoms for which spectral resolution would permit us to distinguish the orbital angular momentum of the upper state. In order to ascertain which excited orbital states are primarily responsible for the observed polarization of the Balmer-α line, a magnetic field has been applied perpendicular to the beam axis and the polarization as a function of field strength has been measured. The half-width of the resultant depolarization curve which is shown in Fig. 7 for a bombarding energy of 50 eV is related to the product of the g factors and the lifetimes of the excited states $g_F\tau$. This quantity is different for each angular momentum state of the $n=3$ level and allows us to determine that the ^2D states are primarily responsible for the polarization near threshold. In principle, such measurements could be refined to reveal which mag-

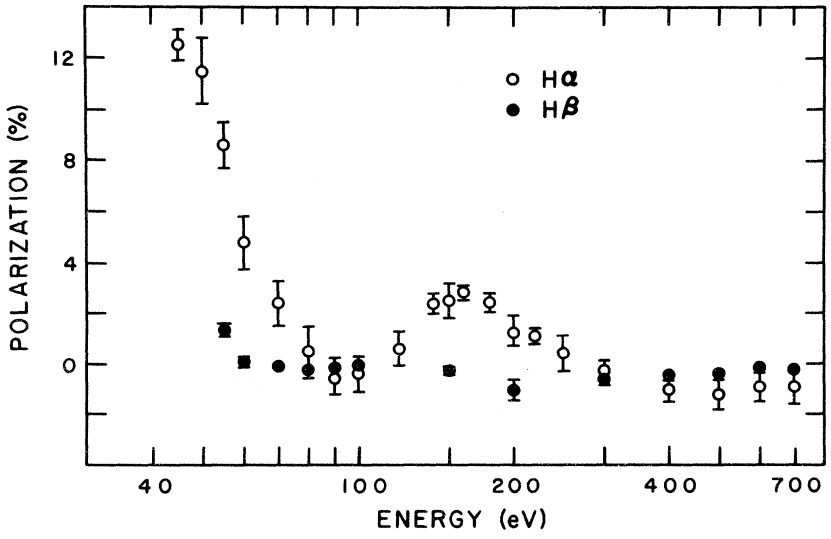

FIG. 6. Polarization of hydrogen lines as a function of ion energy.

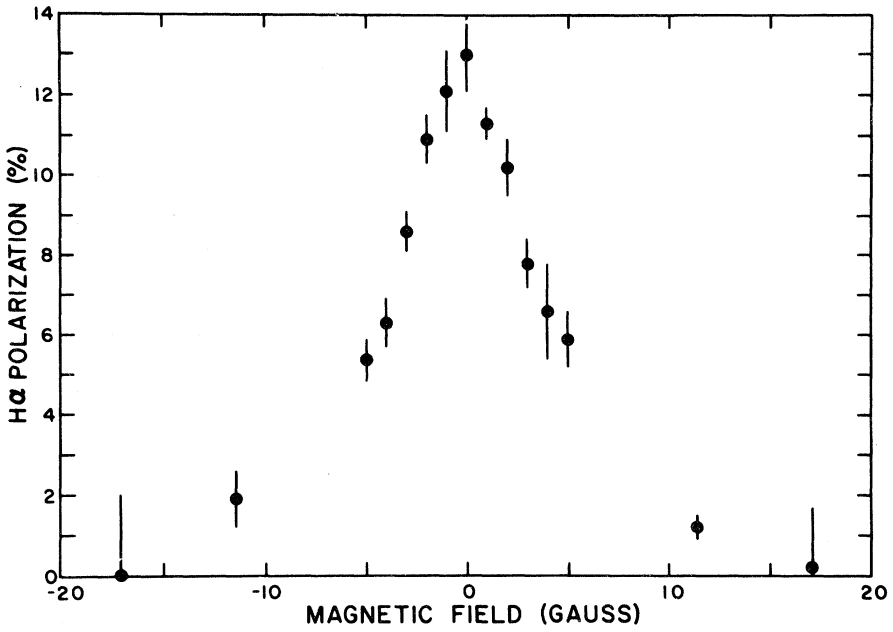

FIG. 7. Polarization of the Balmer-α line produced by 50-eV He^+ ions as a function of magnetic field strength.

netic sublevels are preferentially populated, and, by making the proper correlation of these levels to states of the H_2^+ molecule, to obtain information about the angular distribution of the dissociation axes. Our experiments are not accurate enough to achieve this goal, however, and an additional argument concerning correlation of the orbitals in the separate and united atoms of the H_2^+ molecule is used to infer that the dissociation is peaked perpendicular to the beam axis.

The calculations which relate the polarization of atomic lines to the angular distribution of the dissociation axis is carried out in the Appendix. If both the observation direction and the applied magnetic field are perpendicular to the beam, the polarization for transitions between states described by a completely coupled angular momentum scheme $|(SL)JIFm\rangle$ is given by

$$P=\sum DG_1(\tfrac{1}{2}\Pi)/\sum(B+\tfrac{1}{3}D)\,, \tag{1}$$

where

$$D=(-1)^{S+2F+I+2J-L+m+1}C_2^{L',m_L}(2L+1)(2L'+1)$$
$$\times(2J+1)(2F+1)\tfrac{3}{2}\sqrt{\tfrac{2}{15}}\,A_{\nu n}\begin{pmatrix}L' & L & 1\\ 0 & 0 & 0\end{pmatrix}^2\begin{pmatrix}F & 2 & F\\ m & 0 & -m\end{pmatrix}$$
$$\times\begin{Bmatrix}I & F & J\\ 2 & J & F\end{Bmatrix}\begin{Bmatrix}L' & L & 1\\ 2 & 1 & L\end{Bmatrix}\begin{Bmatrix}S & L & J\\ 2 & J & L\end{Bmatrix}, \tag{2}$$

$$B=C_0^{L',m_L}(2L'+1)\tfrac{2}{3}A_{\nu n}\begin{pmatrix}L' & L & 1\\ 0 & 0 & 0\end{pmatrix}^2, \tag{3}$$

and

$$G_1(\tfrac{1}{2}\pi)=\Gamma^2[\Gamma^2+(2\omega_F)^2]^{-1}\,. \tag{4}$$

The factors C_l^{L',m_L} are coefficients of the lth-order Legendre polynomials in the expansion for the angular distribution.

$$\rho_{mm}^{\prime(F)}=\sum_{l\ \text{even}}C_l^{L',m_L}P_l(\cos\theta)\,. \tag{5}$$

The superscripts L and m_L are the orbital quantum numbers of atomic states which are populated by dissociation from a given molecular state for which $\Lambda=m_L$. Angular momentum quantum numbers which are primed refer to the lower state and those which are unprimed refer to the upper state. The factor $A_{\nu n}$ is the square of the transition integral.

The lifetime of the excited state is given by $\tau=1/\Gamma$ and the Larmor precessional frequency by

$$\omega_F=g_F\mu_B H/\hbar\,. \tag{6}$$

If the collision excites only magnetic substates which have the same value of ω_F then the polarization as a function of magnetic field strength can be written as the product of the polarization at zero field and a Lorentzian curve

$$P(H)=P(0)\Gamma^2[\Gamma^2+(2\omega_F)^2]^{-1}\,. \tag{7}$$

This situation does not usually occur, however, even if only a single dissociative electronic state of the molecule is excited. The various electron spin states and nuclear spin states that can be combined with the electronic state correlate to sublevels of the dissociated hydrogen atom which have differing values of J, F, and m, and the field dependent polarization consists of a sum of Lorentz curves of various amplitudes and widths.

Equations (2) and (3) show explicitly that only the zeroth- and second-order coefficients of the expansion in Eq. (5) appear in the formula for the polarization of electric dipole radiation. Therefore, the full angular dependence of the dissocia-

tion cannot be obtained from optical measurements.

It will be useful to evaluate Eq. (1) for the cases in which only a single electronic state of H_2^+ is excited. In order to proceed with these computations it is necessary to determine the correlation between the molecular states, including electronic and nuclear spin, and the atomic states of hydrogen. Because electrostatic interactions dominate the excitation process it is generally assumed that the spin states are equally populated.

A given Λ state of a molecule can usually be uniquely correlated to states of the separated atom which have definite values of orbital angular momentum, but there is some ambiguity in making this association for H_2^+ because of the near degeneracies of the various orbital states which have the same value of the total quantum number. Thus a σ state might correlate to mixtures of $\sigma 3s$, $\sigma 3p$, and $\sigma 3d$ in the separated atom. The atomic states are not degenerate, of course, owing to the effects of electron spin and the Lamb shifts, and it would be possible to obtain unique adiabatic correlations. Such correlations still do not assure that one knows which states of the atom are populated subsequent to excitation of a given molecular electronic state. The proton and hydrogen atom may be dissociating with several volts excess energy, and the nuclear motion can cause excitation transfer in the region where states of the same symmetry cross. Nevertheless, in order to effect some comparison between the theory of polarization given here and the experimental results, we have assumed the diabatic correlation between molecular orbitals and atomic orbital states shown in Table II. The correlations to specific magnetic substates are obtained by setting $m_L = \pm\Lambda$, taking $m_J = m_L - \frac{1}{2}$ for $J = L - \frac{1}{2}$, $-L+1 \leq m_L \leq L$, and then associating the remaining substates with $J = L + \frac{1}{2}$. The correlation to hyperfine states has been performed in an analogous manner by coupling each magnetic sublevel of the fine-structure multiplet to $m_I = \pm\frac{1}{2}$. The results for the P and D terms (there is no polarization observed from S states) of the $n=3$ level are shown in Table II together with formulas for the polarization if only a single molecular orbital is excited. The quantities β_{L,m_L} are the ratios $C_2^{L,m_L}/C_0^{L,m_L}$ which are taken to be the same for all atomic states which correlate to a given state of H_2^+. These formulas are plotted in Fig. 8 for comparison with the experimental values obtained at an ion energy of 50 eV. The measured points are the average of two symmetrized depolarization curves, and the uncertainties represent the average error at each point. The comparison of experimental and theoretical results shows that the polarization arises almost entirely from $3\,^2D \rightarrow 2\,^2P$ transitions but the experimental errors and the uncertainty of the assumed correlations make it impossible to determine from this data alone which set of atomic hyperfine levels is being preferentially populated.

TABLE II. Correlation of molecular and atomic states and expressions for the polarization in a magnetic field if a single molecular state is excited. The Larmor precession frequencies are designated as $\omega_{J,F}$.

Molecular states	Fine-structure states ($n=3$)	Hyperfine states F	Hyperfine states m_F	Polarization
$4d\sigma_g$, $5f\sigma_u$	$P^{1/2}_{3/2}$	2	1	
		1	0	$\frac{3\Gamma^2\beta_{1,0}}{120+3\beta_{1,0}}\left(\frac{1}{\Gamma^2+(2\omega_{3/2,2})^2}+\frac{2}{\Gamma^2+(2\omega_{3/2,1})^2}\right)$
	$P^{-1/2}_{1/2}$	1	0, −1	
$3p\pi_u$, $4d\pi_g$	$P^{\mp 3/2}_{3/2}$, $P^{-1/2}_{3/2}$	2	2, 0, −1, −2	
		1	1, −1	$\frac{-3\Gamma^2\beta_{1,1}}{120-3\beta_{1,1}}\left(\frac{1}{\Gamma^2+(2\omega_{3/2,2})^2}+\frac{2}{\Gamma^2+(2\omega_{3/2,1})^2}\right)$
	$P^{1/2}_{1/2}$	1	1	
		0	0	
$5g\sigma_g$, $6h\sigma_u$	$D^{1/2}_{5/2}$	3	1	$\frac{3\Gamma^2\beta_{2,0}}{1600+35\beta_{2,1}}\left(\frac{12}{\Gamma^2+(2\omega_{5/2,3})^2}+\frac{16}{\Gamma^2+(2\omega_{5/2,2})^2}\right.$
		2	0	
	$D^{-1/2}_{3/2}$	2	0	$\left.+\frac{14}{\Gamma^2+(2\omega_{3/2,2})^2}-\frac{7}{\Gamma^2+(2\omega_{3/2,1})^2}\right)$
		1	−1	
$4f\pi_u$, $5g\pi_g$	$D^{3/2}_{5/2}$, $D^{-1/2}_{5/2}$	3	2, 0	$\frac{3\Gamma^2\beta_{2,1}}{3200+46\beta_{2,1}}\left(\frac{16}{\Gamma^2+(2\omega_{5/2,3})^2}+\frac{16}{\Gamma^2+(2\omega_{5/2,2})^2}\right.$
		2	1, −1	
	$D^{1/2}_{3/2}$, $D^{-3/2}_{3/2}$	2	1, −1, −2	$\left.+\frac{14}{\Gamma^2+(2\omega_{3/2,1})^2}\right)$
		1	0	
$3d\delta_g$, $4f\delta_u$	$D^{\mp 5/2}_{5/2}$, $D^{-3/2}_{5/2}$	3	3, −1, −2, −3	
		2	2, −2	$\frac{-3\Gamma^2\beta_{2,2}}{3200-81\beta_{2,2}}\left(\frac{28}{\Gamma^2+(2\omega_{5/2,3})^2}+\frac{32}{\Gamma^2+(2\omega_{5/2,2})^2}\right.$
	$D^{3/2}_{3/2}$	2	2	
		1	1	$\left.+\frac{14}{\Gamma^2+(2\omega_{3/2,2})^2}+\frac{7}{\Gamma^2+(2\omega_{3/2,1})^2}\right)$

The fact that the experimental depolarization curve fits so closely to the curves computed for $3\,^2D \rightarrow 2\,^2P$ transitions might have been expected. A comparison of the emission cross sections for H_α and Ly-β at 50 eV shows that they are in the ratio 2/1; the branching ratios for transitions from the $3\,^2P$ state indicate that the probability for decay to the $1\,^2S$ state is almost eight times the probability for decay to the $2\,^2S$ so that less than 7% of the intensity in the Balmer-α line can be due to excitation of the P state. Only if the polarization of the $3\,^2P \rightarrow 2\,^2S$ component were significantly larger than that from the $3\,^2D \rightarrow 2\,^2P$ component would the experimental depolarization curve be broader than the theoretical curves for D-state excitation; such, however, is not the case.

Interpretation of the polarization measurements to obtain information about the angular distribution of dissociation axes of the H_2^+ molecule must rely upon the observation that the emission cross sections listed in Table I and the curves of Fig. 4 show that the probabilities for exciting the various lines of the Lyman and Balmer series decrease as the total quantum number of the upper state increases. This variation with quantum number is most pronounced at low energies; for example, the ratio of the emission cross section of H_β to that of H_α is 0.18 at 700 eV but is only 0.03 at 50 eV. Excited orbitals of a dissociated hydrogen atom correlate to various molecular states which are designated by the quantum numbers $n'L'm_L$ in the united atom (He^+) limit. For the most part, the larger is the total quantum number n of an atomic hydrogen state, the larger is the quantum number n' of the state $|n'L'm_L\rangle$ to which it correlates. The united atom designation is the most appropriate one for characterizing the orbitals of H_2^+,[11] and the decrease of emission rates for the higher members of the hydrogen series implies that the probability

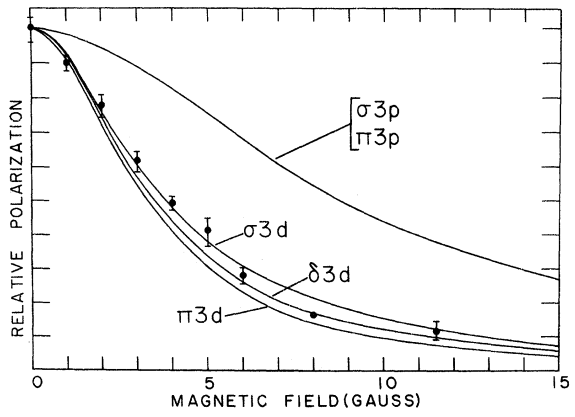

FIG. 8. Comparison of experimental depolarization in magnetic field (solid circles) with theoretical curves calculated from Table II.

of promoting a $1s\sigma$ orbital of H_2 to an excited orbital of H_2^+ simultaneously with charge transfer decreases with increasing values of n'.

Three molecular orbitals with $n'=3$ correlate to the $n=3$ level of the hydrogen atom[12]; these are $3d\delta_g$, $3p\pi_u$, and $3s\sigma_g$. The other nine molecular orbitals which correlate to the $n=3$ level all have $n' \geq 4$. It would appear that the polarization of the H_α line at low collision energies is due to the preferential excitation of the $n'=3$ levels and subsequent dissociation which produces unequal populations of the magnetic sublevels of the $3\,^2D$ state. As the ion energy is increased, the $n'=4$ and 5 levels are excited more readily and the populations of the magnetic substates become more nearly equal thus reducing the polarization of the H_α line. Now the $3d\delta_g$ state can dissociate only into $3\,^2D$ states of the hydrogen atom which in a strong field have $m_L = \pm 2$. The $3p\pi_u$ and $3s\sigma_g$ states dissociate into levels which have $m_L = \pm 1$ or $m_L = 0$, respectively; these states would correlate to $3\,^2P$ and $3\,^2S$ in the absence of an external electric field if the terms of the $n=3$ level were well separated in energy and ordered according to increasing orbital angular momentum. However, as noted previously, the correlation is somewhat uncertain and it is possible that a fraction of the molecules excited into $3p\pi_u$ state may dissociate into the $3\,^2D_{3/2}$ state. From Table II, it is seen that for equal values of the excitation cross section and the parameter β that the largest contribution to the polarization comes from preferential population of the δ state. If we assume that only the ^2D atomic levels which correlate to this state are significantly populated at a collision energy of 50 eV the value of β is calculated (taking the fractional polarization to be 0.12) to be equal to -1.6. The angular distribution then becomes

$$\rho'_{22}(\theta) \sim 1.8 - 2.4\cos^2\theta + (\text{higher-order terms}) . \tag{8}$$

Although the higher-order terms in Eq. (8) cannot be assumed as negligible [the coefficients must add to at least 0.6 if $\rho'_{22}(\theta)$ is to be positive at $\theta = 0$], the first two terms indicate that the excitation of the H_2^+ molecule takes place most probably if the internuclear axis is perpendicular to the beam axis.

McKnight[13] has recently reported direct measurements of the angular distribution from 1–5 keV of atomic metastables produced by the reaction we have studied here. His results indicate that there is very little momentum transfer and indeed show a distribution in the laboratory reference frame similar to that which is indicated by our analysis of the optical results; namely, the metastables are emitted with a distribution that is peaked at right angles to the beam. When the momentum

transfer is very small the angular distribution of fragments from a dissociating state of H_2^+ should be the same as the angular distribution of the dissociation axis. Therefore, both the optical polarization experiments and the measurements of metastable hydrogen atoms qualitatively indicate the same angular dependence of the dissociative charge-exchange reaction from the $He^+ + H_2$ system.

APPENDIX: POLARIZATION CALCULATIONS

The intensity of light radiated from transitions between hyperfine states can be expressed as a summation over the radiation of all the sublevels. If the states are expressed in a coupled scheme, we have

$$I \sim \sum_{\Phi F, \alpha\beta\mu} \langle \nu\Phi\mu | \vec{e}\cdot\vec{r} | nF\alpha \rangle \langle \rho^{(F)}_{\alpha\beta}(t) \rangle \times \langle nF\beta | \vec{e}\cdot\vec{r} | \nu\Phi\mu \rangle , \quad \text{(A1)}$$

where Φ and F are the total-angular-momentum quantum numbers, respectively, of the lower and upper levels of the transition; μ, α, and β are the magnetic quantum numbers of the sublevels; and ν and n specify all quantum numbers associated with the radial wave functions. The relative populations of the sublevels excited by collisions are not known but are specified by the time-dependent elements of an excitation matrix of rank F, $\rho^{(F)}_{mm'}(t)$.[14] These elements are functions of the orientation of the dissociation axis and must be averaged over the angular distribution.

Measurements of linear polarization are made parallel and perpendicular to the beam axis so we choose to calculate the matrix elements with reference to a coordinate system which has its z axis aligned along the beam. The spherical tensor operators $rC_0^{(1)}$ and $r(C_{-1}^{(1)} - C_1^{(1)})/\sqrt{2}$ are used to calculate the matrix elements appropriate to $I_\parallel$ and $I_\perp$, respectively, and the polarization is defined as

$$P = \frac{I_\parallel - I_\perp}{I_\parallel + I_\perp} . \quad \text{(A2)}$$

The excitation matrix is diagonal with respect to a coordinate system in which the z axis is aligned along the dissociation axis, i.e., along the internuclear axis of the excited H_2^+ molecule. It is along this axis that the projection of electronic orbital angular momentum are quantized to form the various Λ states of the molecule. Upon dissociation these states (including electron and nuclear spins) correlate to states $|nSLJFm\rangle$ of the excited atom for which $m_L = \Lambda$. The relative populations of the states produced by the collision is not known *a priori*; as we have noted, the depolarization experiments have been made in an attempt to determine which of these states may be selectively populated. The excitation matrices in the two coordinate systems are related by the expression[15]

$$\rho^{(F)}_{\kappa\lambda} = \sum_m D^{(F)}_{m\kappa}(\phi, \theta, \gamma)\, \rho'^{(F)}_{mm} D^{(F)}_{m\lambda}{}^*(\phi, \theta, \gamma) , \quad \text{(A3)}$$

where $\rho'^{(F)}_{mm}$ is an element of the diagonal excitation matrix and the D's are elements of the rotation matrix which relate the excitation matrices in the the two coordinate systems by rotation through the Euler angles ϕ, θ, and γ. Because the angular distribution of the dissociation axis is symmetric around the beam axis, we can express it as an expansion in Legendre polynomials,

$$\rho'^{(F)}_{mm} = \sum_l C_l^{L,m_L} P_l(\cos\theta) , \quad \text{(A4a)}$$

or in terms of the elements of the rotation matrix,

$$\rho'^{(F)}_{mm} = \sum_l C_l^{L,m_L} D^{(l)}_{00}(\phi, \theta, \gamma) , \quad \text{(A4b)}$$

where the C's are constant coefficients, and the superscripts L and m_L are the orbital quantum numbers of the atomic states which are populated by dissociation from a given molecular electronic state. The average of $\rho^{(F)}_{\kappa\lambda}$ over the rotation angles is then

$$\langle \rho^{(F)}_{\kappa\lambda} \rangle = \sum_{lm} (-1)^{m-\lambda} C_l^{L,m_L} \int_0^{2\pi}\int_0^{\pi}\int_0^{2\pi} D^{(F)}_{m\kappa}(\phi, \theta, \gamma) \times D^{(l)}_{00}(\phi, \theta, \gamma)\, D^{(F)}_{-m-\gamma}(\phi, \theta, \gamma)\, d\phi \sin\theta\, d\theta\, d\gamma , \quad \text{(A5)}$$

$$\langle \rho^{(F)}_{\kappa\lambda} \rangle = \sum_{lm} (-1)^{m-\lambda} C_l^{L,m_L} \begin{pmatrix} F & l & F \\ m & 0 & -m \end{pmatrix} \begin{pmatrix} F & l & F \\ \kappa & 0 & -\lambda \end{pmatrix} .$$

The 3-j symbols have nonzero values only if the sum of the elements in the bottom row vanishes so that $\kappa = \lambda$. If there is no magnetic field present in the collision region, Eq. (A5) can be used in (A1) by setting $\kappa = \lambda = \alpha = \beta$.

When a uniform magnetic field is applied to the collision chamber in an arbitrary direction, the density matrix is obtained from solutions of the differential equation

$$\dot{\rho}'' = -(i/\hbar)[\mathcal{H}, \rho''] - \rho''\Gamma + \rho^{0\prime\prime} R_P . \quad \text{(A6)}$$

The term $\rho^{0\prime\prime} R_P$ represents the steady-state rate at which elements of the excitation matrix are generated by collisions. The temporal evolution subsequent to excitation is given by the commutator of ρ'' with the Hamiltonian for the system and by the radiative decay rate $\rho''\Gamma$. For application of Eq. (A6) to the present problem, only that part of $\mathcal{H}$ which describes the interaction of excited states with the external field is of interest and for a given element of ρ'' we can write

$$\dot{\rho}''^{(F)}_{\gamma\delta} = -i\omega_F(\gamma - \delta)\rho_{\gamma\delta} - \Gamma\rho''_{\gamma\delta} + R_P\rho^{0\prime\prime}_{\gamma\delta} , \quad \text{(A7)}$$

where γ and δ are the magnetic quantum numbers of the excited states. The quantity ω_F[16] is the Larmor precessional frequency given by

$$\omega_F = g_F \mu_B H/\hbar\,, \tag{A8}$$

where g_F is the g factor for the state and H is the magnetic field strength. Equation (A7) is obtained by evaluating the operator for the Zeeman effect in a coordinate system which has a quantization axis in the direction of the magnetic field so that we obtain uncoupled differential equations for the elements of ρ''. The steady-state solution of Eq. (A7) is

$$\rho''_{\gamma\delta} = R_P \rho^{0\prime\prime}_{\gamma\delta} [\Gamma + i(\gamma-\delta)\omega_F]^{-1}\,. \tag{A9}$$

In order to obtain the elements $\rho^{(F)}_{\alpha\beta}$ of Eq. (1), $\rho^{0\prime\prime}_{\gamma\delta}$ must be computed and the elements $\rho_{\alpha\beta}$, which are referred to the coordinate system in which the z axis is aligned along the beam, must be expressed in terms of the elements $\rho''_{\gamma\delta}$ which have been calculated for a coordinate system in which the z axis is aligned with the magnetic field. From Eq. (A2) we obtain

$$\rho^{0\prime\prime}_{\gamma\delta} = \sum_{m\kappa\lambda} D^{(F)}_{\gamma\kappa}{}^*(\omega) D^{(F)}_{m\kappa}(\phi,\theta,\gamma)\rho'^{(F)}_{mm} \times D^{(F)}_{m\lambda}{}^*(\phi,\theta,\gamma) D^{(F)}_{\delta\lambda}(\omega)\,, \tag{A10}$$

where ω denotes the three Euler angles 0, ψ, and Ω, and ψ and Ω themselves are the polar and azimuthal angles of the field direction. Also, we have

$$\rho^{(F)}_{\alpha\beta} = \sum_{\gamma\delta} D^{(F)}_{\gamma\alpha}(\omega)\rho^{(F)\prime\prime}_{\gamma\delta} D^{(F)}_{\delta\beta}{}^*(\omega)\,. \tag{A11}$$

Equation (A1) becomes

$$I \sim \sum_{\substack{F\Phi m\mu\\ \alpha\beta\kappa\lambda\gamma\delta}} \langle \nu\Phi\mu|\vec{\epsilon}\cdot\vec{r}|nF\alpha\rangle\langle\nu F\beta|\vec{\epsilon}\cdot\vec{r}|\nu\Phi\mu\rangle[\Gamma+i(\gamma-\delta)\omega_F]^{-1} \times D^{(F)}_{\gamma\alpha}(\omega) D^{(F)}_{\gamma\kappa}{}^*(\omega)\langle D^{(F)}_{m\kappa}(\phi,\theta,\gamma)\rho'^{(F)}_{mm} D^{(F)}_{m\lambda}{}^*(\phi,\theta,\gamma)\rangle D^{(F)}_{\delta\lambda}(\omega) D^{(F)}_{\delta\beta}{}^*(\omega)\,. \tag{A12}$$

The average over the angular distribution of the dissociation axes has already been obtained in Eq. (A5). After applying the Wigner-Eckart theorem to the matrix elements for the dipole operator the expressions for the intensities of light polarized parallel to the perpendicular to the beam axes are

$$I_\parallel \sim \sum_{\substack{F\Phi m\mu\\ \kappa\gamma\delta l}} (-1)^{\Phi+F+m+\gamma+\delta-2\kappa-3\mu} C^{L,m_L}_l |\langle n|r|\nu\rangle|^2 \langle\Phi||C^{(1)}||F\rangle\langle F||C^{(1)}||\Phi\rangle \times \begin{pmatrix}\Phi & 1 & F\\ -\mu & 0 & \mu\end{pmatrix}^2 \begin{pmatrix}F & l & F\\ m & 0 & -m\end{pmatrix}\begin{pmatrix}F & l & F\\ \kappa & 0 & -\kappa\end{pmatrix} [\Gamma+i(\gamma-\delta)\omega_F]^{-1} D^{(F)}_{\gamma\mu}(\omega) D^{(F)}_{-\gamma-\kappa}(\omega) D^{(F)}_{\delta\kappa}(\omega) D^{(F)}_{-\delta-\mu}(\omega)\,, \tag{A13a}$$

$$I_\perp \sim \sum_{\substack{F\Phi m\mu\\ \kappa\gamma\delta l}} (-1)^{\Phi+F+m-\kappa-2\mu-1} C^{L,m_L}_l |\langle n|r|\nu\rangle|^2 \langle\Phi||C^{(1)}||F\rangle\langle F||C^{(1)}||\Phi\rangle \begin{pmatrix}F & l & F\\ m & 0 & -m\end{pmatrix}\begin{pmatrix}F & l & F\\ \kappa & 0 & -\kappa\end{pmatrix} \times [\Gamma+i(\gamma-\delta)\omega_F]^{-1}\Bigg[\begin{pmatrix}\Phi & 1 & F\\ -\mu & -1 & \mu+1\end{pmatrix}\begin{pmatrix}F & 1 & \Phi\\ -\mu+1 & -1 & \mu\end{pmatrix}[(-1)^{\gamma+\delta-\kappa-\mu+1} D^{(F)}_{\gamma,\mu+1}(\omega) D^{(F)}_{-\gamma-\kappa}(\omega) D^{(F)}_{\delta\kappa}(\omega) \times D^{(F)}_{-\delta,-\mu+1}(\omega) + (-1)^{\gamma+\delta-\kappa-\mu-1} D^{(F)}_{\gamma,\mu-1}(\omega) D^{(F)}_{-\gamma,-\kappa}(\omega) D^{(F)}_{\delta\kappa}(\omega) D^{(F)}_{-\delta,-\mu-1}(\omega)] - \begin{pmatrix}\Phi & 1 & F\\ -\mu & -1 & \mu+1\end{pmatrix}\begin{pmatrix}F & 1 & \Phi\\ -\mu-1 & 1 & \mu\end{pmatrix}[(-1)^{\gamma+\delta-\kappa-\mu-1} D^{(F)}_{\gamma,\mu+1}(\omega) D^{(F)}_{-\gamma-\kappa}(\omega) D^{(F)}_{\delta\kappa}(\omega) D^{(F)}_{-\delta,-\mu-1}(\omega) + (-1)^{\gamma+\delta-\kappa-\mu+1} D^{(F)}_{\gamma,\mu-1}(\omega) D^{(F)}_{-\gamma,-\kappa}(\omega) D^{(F)}_{\delta\kappa}(\omega) D^{(F)}_{-\delta,-\mu+1}(\omega)]\Bigg]\,. \tag{A13b}$$

It is now useful to change the summation indices so that terms which correspond to different values of $(\gamma-\delta)$ can be treated separately. By letting $(\gamma-\delta)=\sigma$ and utilizing the orthogonality properties of the 3-j symbols we obtain

$$I_\parallel \sim \sum_{\substack{\Phi F\\ m\mu\sigma l}} (-1)^{\Phi+3F+m-\sigma-3\mu+l} C^{L,m_L}_l A_{\nu\eta}\langle\Phi||C^{(1)}||F\rangle\langle F||C^{(1)}||\Phi\rangle \times \begin{pmatrix}\Phi & 1 & F\\ -\mu & 0 & \mu\end{pmatrix}^2 \begin{pmatrix}F & F & l\\ \mu & -\mu & 0\end{pmatrix}\begin{pmatrix}F & l & F\\ m & 0 & -m\end{pmatrix} D^{(l)}_{-\sigma 0}(\omega) D^{(l)}_{\sigma 0}(\omega)(\Gamma+i\sigma\omega_F)^{-1}\,, \tag{A14}$$

where $A_{\nu\eta} = |\langle n|r|\nu\rangle|^2$. The summation over μ yields

$$I_\parallel \sim \sum_{\substack{\Phi F\\ m\sigma l}} (-1)^{3F+m-\sigma+l} C^{L,m_L}_l A_{\nu\eta}\langle\Phi||C^{(1)}||F\rangle\langle F||C^{(1)}||\Phi\rangle \times \begin{pmatrix}1 & 1 & l\\ 0 & 0 & 0\end{pmatrix}\begin{Bmatrix}1 & 1 & l\\ F & F & \Phi\end{Bmatrix}\begin{pmatrix}F & l & F\\ m & 0 & -m\end{pmatrix} D^{(l)}_{-\sigma 0}(\omega) D^{(l)}_{\sigma 0}(\omega)(\Gamma+i\sigma\omega_F)^{-1}\,. \tag{A15}$$

The first 3-j symbol in Eq. (A15) must satisfy a triangular condition $\Delta(11L)$ in order to be nonzero; also its symmetry properties require that it vanish for $l=1$. These conditions restrict the values of l to $l=0$, 2 and imply that $\sigma=0$, 1, 2 only. The analogous result for radiation perpendicular to the beam axis is

$$I_\perp \sim \sum_{\substack{\Phi F \\ m\sigma l}} (-1)^{3F+m-\sigma} C_l^{L,m_L} A_{\nu n} \langle \Phi || C^{(1)} || F \rangle \langle F || C^{(1)} || \Phi \rangle [\Gamma + i\sigma\omega_F]^{-1} \begin{pmatrix} F & l & F \\ m & 0 & -m \end{pmatrix} \begin{Bmatrix} 1 & 1 & l \\ F & F & \Phi \end{Bmatrix}$$
$$\times \left[-\begin{pmatrix} 1 & 1 & l \\ 1 & -1 & 0 \end{pmatrix} D^{(1)}_{\sigma 0}(\omega) D^{(1)}_{-\sigma 0}(\omega) + \frac{1}{2} \begin{pmatrix} 1 & 1 & l \\ -1 & -1 & 2 \end{pmatrix} [D^{(1)}_{-\sigma 0}(\omega) D^{(1)}_{\sigma 2}(\omega) + D^{(1)}_{-\sigma 0}(\omega) D^{(1)}_{\sigma -2}(\omega)] \right] \quad \text{(A16)}$$

and the same restrictions apply to l and σ as noted for $I_\parallel$. These restrictions limit the information which can be obtained about the angular distribution because only C_0^{L,m_L} and C_2^{L,m_L} appear in the result. The polarization from electric dipole radiation, when averaged over the angular distribution of the dissociation axes, cannot provide information about any terms in the angular distribution, Eq. (A4), which are of higher order than the dipolar term. This limitation does not depend on our choice of observation axes to obtain $I_\parallel$ and $I_\perp$.

After substituting explicit values for the D's in Eqs. (A15) and (A16), the following expressions are obtained for the polarization intensities:

$$I_\parallel \sim \sum_{\Phi F m} (-1)^{3F+m} A_{\nu n} \langle \Phi || C^{(1)} || F \rangle \langle F || C^{(1)} || \Phi \rangle \left[-C_0^{L,m_L} \sqrt{\tfrac{1}{3}} \begin{Bmatrix} 1 & 1 & 0 \\ F & F & \Phi \end{Bmatrix} \begin{pmatrix} F & 0 & F \\ m & 0 & -m \end{pmatrix} \right.$$
$$\left. + C_2^{L,m_L} \sqrt{\tfrac{2}{15}} \begin{Bmatrix} 1 & 1 & 2 \\ F & F & \Phi \end{Bmatrix} \begin{pmatrix} F & 2 & F \\ m & 0 & -m \end{pmatrix} \left(\tfrac{1}{4}(2\cos^2\psi - \sin^2\psi)^2 + \frac{3\Gamma^2 \cos^2\psi \sin^2\psi}{\Gamma^2 + \omega_F^2} + \frac{3}{4} \frac{\Gamma^2 \sin^4\psi}{\Gamma^2 + (2\omega_F)^2} \right) \right], \quad \text{(A17a)}$$

$$I_\perp \sim \sum_{F \Phi m} (-1)^{3F+m} A_{\nu n} \langle \Phi || C^{(1)} || F \rangle \langle F || C^{(1)} || \Phi \rangle \left[-C_0^{L,m_L} \sqrt{\tfrac{1}{3}} \begin{Bmatrix} 1 & 1 & 0 \\ F & F & \Phi \end{Bmatrix} \begin{pmatrix} F & 0 & F \\ m & 0 & -m \end{pmatrix} \right.$$
$$\left. - C_2^{L,m_L} \tfrac{1}{2} \sqrt{\tfrac{2}{15}} \begin{Bmatrix} 1 & 1 & 2 \\ F & F & \Phi \end{Bmatrix} \begin{pmatrix} F & 2 & F \\ m & 0 & -m \end{pmatrix} \left(\tfrac{1}{2}(3\cos^2\psi - 1) + \frac{3}{2} \frac{\Gamma^2 \sin^2\psi}{\Gamma^2 + (2\omega F)^2} \right) \right]. \quad \text{(A17b)}$$

Equation (A17a) and (A17b) show that the intensities of light observed parallel to and perpendicular to the ion beam are independent of the azimuthal angle of the field and depend only upon the polar angle ψ.

The reduced matrix elements are evaluated for an L-S coupling scheme

$$\langle SL'J'I\Phi || C^{(1)} || SLJIF \rangle \langle SLJIF || C^{(1)} || SL'J'I\Phi \rangle = (-1)^{2J+2J'+2S+2I+L'+L+F+\Phi+1} (2\Phi+1)(2F+1)$$
$$\times (2J'+1)(2J+1)(2L'+1)(2L+1) \begin{Bmatrix} J' & \Phi & I \\ F & J & 1 \end{Bmatrix}^2 \begin{Bmatrix} L' & J' & S \\ J & L & 1 \end{Bmatrix}^2 \begin{pmatrix} L' & 1 & L \\ 0 & 0 & 0 \end{pmatrix}^2, \quad \text{(A18)}$$

where the primed quantum numbers refer to the lower state of the transition. Finally, summation over Φ and J' yields an expression for the polarization,

$$P = \sum DG_1(\psi) / \sum [B + \tfrac{1}{3} DG_2(\psi)], \quad \text{(A19)}$$

with

$$D = (-1)^{S+2F+I+2J-L+m+1} C_2^{L,m_L} (2L+1)(2L'+1)(2J+1)(2F+1)$$
$$\times \tfrac{3}{2} \sqrt{\tfrac{2}{15}} A_{\nu n} \begin{pmatrix} L' & L & 1 \\ 0 & 0 & 0 \end{pmatrix}^2 \begin{pmatrix} F & 2 & F \\ m & 0 & -m \end{pmatrix} \begin{Bmatrix} I & F & J \\ 2 & J & F \end{Bmatrix} \begin{Bmatrix} L' & L & 1 \\ 2 & 1 & L \end{Bmatrix} \begin{Bmatrix} S & L & J \\ 2 & J & L \end{Bmatrix}, \quad \text{(A20)}$$

$$B = C_0^{L,m_L} (2L'+1) \tfrac{2}{3} A_{\nu n} \begin{pmatrix} L' & L & 1 \\ 0 & 0 & 0 \end{pmatrix}^2, \quad \text{(A21)}$$

$$G_1(\psi) = \frac{1}{2} \left(\cos^2\psi (2 - 3\sin^2\psi) + \frac{4\Gamma^2 \cos^2\psi \sin^2\psi}{\Gamma^2 + (\omega_F)^2} + \frac{\Gamma^2 \sin^2\psi (\sin^2\psi + 1)}{\Gamma^2 + (2\omega_F)^2} \right), \quad \text{(A22)}$$

$$G_2(\psi) = \frac{1}{2} \left(2 - 9\sin^2\psi \cos^2\psi + \frac{12\Gamma^2 \sin^2\psi \cos^2\psi}{\Gamma^2 + (\omega_F)^2} - \frac{3\Gamma^2 \sin^2\psi \cos^2\psi}{\Gamma^2 + (2\omega_F)^2} \right). \quad \text{(A23)}$$

At an observation angle of $\psi = 90°$ $G_2(\psi)$ is equal to unity and $G_1(\psi)$ is equal to $\Gamma^2[\Gamma^2 + (2\omega_F)^2]^{-1}$. The summation indices in Eq. (A19) are taken over all states which are not resolved optically, usually the hyperfine or fine structure states. Also, it should be noted that the ω_F's which appear in Eqs. (A22)

and (A23) depend upon which fine structure component is being considered because the g factor is given by

$$g_F = g_J\left(\frac{F(F+1)+J(J+1)-I(I+1)}{2F(F+1)}\right). \quad \text{(A24)}$$

†Work partially supported by a grant from the National Aeronautics and Space Administration.

[1]J. B. H. Stedeford and J. B. Hasted, Proc. Roy. Soc. (London) A227, 474 (1954).

[2]G. H. Dunn, R. Geballe, and D. Pretzer, Phys. Rev. 128, 2200 (1962); G. H. Dunn, R. Geballe, and D. Pretzer, in *Proceedings of the Second International Conference on the Physics of Electronic and Atomic Collisions, Boulder, Colorado*, 1961 (Benjamin, New York, 1961), p. 26.

[3]V. A. Gusev, G. N. Polyakova, V. F. Erko, Ya. M. Fogel, and A. V. Zats, in *Abstracts of the Sixth International Conference on the Physics of Electronic and Atomic Collisions* (MIT Press, Cambridge, Mass., 1969), p. 809.

[4]R. D. Nathan and R. C. Isler, Phys. Rev. Letters 26, 1091 (1971).

[5]R. J. Van Brunt and R. N. Zare, J. Chem. Phys. 48, 4304 (1968).

[6]W. L. Wiese, M. W. Smith, and B. M. Glennon, *Atomic Transition Probabilities*, Natl. Bur. Std. Ref. Data Ser. 4 (U.S. GPO, Washington, D.C., 1966), Vol. 1.

[7]R. A. Young, R. F. Stebbings, J. W. McGowan, Phys. Rev. 171, 85 (1968).

[8]F. T. Smith, H. H. Fleischmann, and R. A. Young, Phys. Rev. A 2, 379 (1970).

[9]W. R. Ott, W. E. Kauppila, and W. L. Fite, Phys. Rev. A 1, 1089 (1970); D. A. Vroom and F. J. DeHeer, J. Chem. Phys. 50, 580 (1969).

[10]W. E. Kauppila, P. J. O. Teubner, W. L. Fite, and R. J. Girnius, Phys. Rev. A 2, 1759 (1970).

[11]D. R. Bates, K. Ledsham, and A. L. Stewart, Phil. Trans. Roy. Soc. London A246, 215 (1954).

[12]M. Kotani, K. Ohno, and K. Kayama, *Handbuch der Physik* (Springer, Berlin, 1961), Vol. XXXVII/II, p. 56; P. M. Morse and E. C. G. Stueckelberg, Phys. Rev. 33, 932 (1929).

[13]R. H. McKnight, Bull. Am. Phys. Soc. 16, 1355 (1971).

[14]The excitation matrix is taken to be diagonal in F because we are concerned here only with zero field level crossings. The observation of high-field crossings between sublevels of different total angular momentum states may prove to be useful in determining populations of substates or to be necessary for precise fits to depolarization curves, but the accuracy of the current measurements do not warrant consideration of these factors in the present development.

[15]A. R. Edmonds, *Angular Momentum in Quantum Mechanics*, 2nd ed. (Princeton U.P., Princeton, New Jersey, 1960).

[16]The form of Eq. (7) assumes that the energies of the magnetic sublevels are linear functions of the external field strength; i.e., that F, or in the limit of complete nuclear decoupling J, is a good quantum number. In the intermediate field case, the energies must be computed by diagonalizing the matrix for the Zeeman effect.

PHYSICAL REVIEW A VOLUME 6, NUMBER 3 SEPTEMBER 1972

Photoionization Accompanied by Excitation of Fe I†

Hugh P. Kelly
Department of Physics, University of Virginia, Charlottesville, Virginia 22901
(Received 7 April 1972)

The author has calculated contributions to the total photoionization cross section of Fe I in which the remaining Fe II ion is left in a low-lying excited state. The excited states considered are $(3d)^7\,{}^4P$, ${}^4F$ and $(3d)^6\,{}^5D\,4p\,{}^6D$, ${}^6F$, ${}^6P$, ${}^4F$, ${}^4D$, and ${}^4P$. We used the velocity form for the dipole-matrix elements and calculated the cross sections by means of many-body perturbation theory. Our results are compared with the cross section for photoionization of Fe I without excitation which we calculated recently. Near threshold the contributions to the total photoionization cross section involving excited $(3d)^7$ and $(3d)^6\,{}^5D\,4p$ excited states of Fe I are approximately 20% of the cross section without excitation.

I. INTRODUCTION

Atomic photoionization cross sections are very useful in probing the details of atomic structure and they are also of importance in other areas of physics, particularly astrophysics.[1] It is important for the atomic theorist to be able to make accurate *a priori* calculations of atomic photo-cross-sections. When accurate experimental cross sections exist, the calculations serve as a test of atomic theories and methods of calculation. Once an accurate method of calculation has been established, it can be used to predict cross sections for those cases where experimental results do not yet exist.[1]

Recently we have calculated the photoionization cross section of the neutral iron atom from threshold to 10 keV.[2] The calculation was motivated both by its usefulness for astrophysics[3] and also as an